SLAC-PUB-8531
BABAR-CONF-00/09
hep-ex/0008053
August, 2000

Measurement of the B^0 meson properties using partially reconstructed B^0 to $D^{*-}\pi^+$ and B^0 to $D^{*-}\ell^+\nu_\ell$ decays with the *BABAR* detector

The *BABAR* Collaboration

Abstract

The two B^0 decay processes $B^0 \to D^{*-}\pi^+$ and $B^0 \to D^{*-}\ell^+\nu_\ell$ have been studied by means of a partial reconstruction technique using a data sample collected with the *BABAR* detector at the PEP-II storage ring. To increase statistics, only the soft π^- from the decay $D^{*-} \to \pi^- D^0$ was used in association with either an oppositely-charged high-momentum pion or lepton. Events were then identified by exploiting the constraints from the simple kinematics of $\Upsilon(4S)$ decays. A clear signature is obtained in each case. The position of the B^0 decay point was obtained from the reconstructed $\pi^+(\ell^+)\pi^-$ vertex. The position of the other $\overline{B}^0$ in the event was also determined. Taking advantage of the boost given to the $\Upsilon(4S)$ system by the asymmetric beam energies of PEP-II, the lifetime of the B^0 meson has been measured from the separation distance between the two vertices along the beam direction. The preliminary results are:

$$\tau_{B^0} = 1.55 \pm 0.05 \pm 0.07 \text{ ps},$$
$$\tau_{B^0} = 1.62 \pm 0.02 \pm 0.09 \text{ ps},$$

respectively for the $B^0 \to D^{*-}\pi^+$ and $B^0 \to D^{*-}\ell^+\nu_\ell$ channels.

Submitted to the 30th International Conference on High Energy Physics,
7/27/2000—8/2/2000, Osaka, Japan

Stanford Linear Accelerator Center, Stanford University, Stanford, CA 94309

Work supported in part by Department of Energy contract DE-AC03-76SF00515.

The *BABAR* Collaboration

B. Aubert, A. Boucham, D. Boutigny, I. De Bonis, J. Favier, J.-M. Gaillard, F. Galeazzi, A. Jeremie, Y. Karyotakis, J. P. Lees, P. Robbe, V. Tisserand, K. Zachariadou

Lab de Phys. des Particules, F-74941 Annecy-le-Vieux, CEDEX, France

A. Palano

Università di Bari, Dipartimento di Fisica and INFN, I-70126 Bari, Italy

G. P. Chen, J. C. Chen, N. D. Qi, G. Rong, P. Wang, Y. S. Zhu

Institute of High Energy Physics, Beijing 100039, China

G. Eigen, P. L. Reinertsen, B. Stugu

University of Bergen, Inst. of Physics, N-5007 Bergen, Norway

B. Abbott, G. S. Abrams, A. W. Borgland, A. B. Breon, D. N. Brown, J. Button-Shafer, R. N. Cahn, A. R. Clark, Q. Fan, M. S. Gill, S. J. Gowdy, Y. Groysman, R. G. Jacobsen, R. W. Kadel, J. Kadyk, L. T. Kerth, S. Kluth, J. F. Kral, C. Leclerc, M. E. Levi, T. Liu, G. Lynch, A. B. Meyer, M. Momayezi, P. J. Oddone, A. Perazzo, M. Pripstein, N. A. Roe, A. Romosan, M. T. Ronan, V. G. Shelkov, P. Strother, A. V. Telnov, W. A. Wenzel

Lawrence Berkeley National Lab, Berkeley, CA 94720, USA

P. G. Bright-Thomas, T. J. Champion, C. M. Hawkes, A. Kirk, S. W. O'Neale, A. T. Watson, N. K. Watson

University of Birmingham, Birmingham, B15 2TT, UK

T. Deppermann, H. Koch, J. Krug, M. Kunze, B. Lewandowski, K. Peters, H. Schmuecker, M. Steinke

Ruhr Universität Bochum, Inst. f. Experimentalphysik 1, D-44780 Bochum, Germany

J. C. Andress, N. Chevalier, P. J. Clark, N. Cottingham, N. De Groot, N. Dyce, B. Foster, A. Mass, J. D. McFall, D. Wallom, F. F. Wilson

University of Bristol, Bristol BS8 lTL, UK

K. Abe, C. Hearty, T. S. Mattison, J. A. McKenna, D. Thiessen

University of British Columbia, Vancouver, BC, Canada V6T 1Z1

B. Camanzi, A. K. McKemey, J. Tinslay

Brunel University, Uxbridge, Middlesex UB8 3PH, UK

V. E. Blinov, A. D. Bukin, D. A. Bukin, A. R. Buzykaev, M. S. Dubrovin, V. B. Golubev, V. N. Ivanchenko, A. A. Korol, E. A. Kravchenko, A. P. Onuchin, A. A. Salnikov, S. I. Serednyakov, Yu. I. Skovpen, A. N. Yushkov

Budker Institute of Nuclear Physics, Siberian Branch of Russian Academy of Science, Novosibirsk 630090, Russia

A. J. Lankford, M. Mandelkern, D. P. Stoker

University of California at Irvine, Irvine, CA 92697, USA

A. Ahsan, K. Arisaka, C. Buchanan, S. Chun

University of California at Los Angeles, Los Angeles, CA 90024, USA

J. G. Branson, R. Faccini,[1] D. B. MacFarlane, Sh. Rahatlou, G. Raven, V. Sharma

University of California at San Diego, La Jolla, CA 92093, USA

C. Campagnari, B. Dahmes, P. A. Hart, N. Kuznetsova, S. L. Levy, O. Long, A. Lu, J. D. Richman, W. Verkerke, M. Witherell, S. Yellin

University of California at Santa Barbara, Santa Barbara, CA 93106, USA

J. Beringer, D. E. Dorfan, A. Eisner, A. Frey, A. A. Grillo, M. Grothe, C. A. Heusch, R. P. Johnson, W. Kroeger, W. S. Lockman, T. Pulliam, H. Sadrozinski, T. Schalk, R. E. Schmitz, B. A. Schumm, A. Seiden, M. Turri, D. C. Williams

University of California at Santa Cruz, Institute for Particle Physics, Santa Cruz, CA 95064, USA

E. Chen, G. P. Dubois-Felsmann, A. Dvoretskii, D. G. Hitlin, Yu. G. Kolomensky, S. Metzler, J. Oyang, F. C. Porter, A. Ryd, A. Samuel, M. Weaver, S. Yang, R. Y. Zhu

California Institute of Technology, Pasadena, CA 91125, USA

R. Aleksan, G. De Domenico, A. de Lesquen, S. Emery, A. Gaidot, S. F. Ganzhur, G. Hamel de Monchenault, W. Kozanecki, M. Langer, G. W. London, B. Mayer, B. Serfass, G. Vasseur, C. Yeche, M. Zito

Centre d'Etudes Nucléaires, Saclay, F-91191 Gif-sur-Yvette, France

S. Devmal, T. L. Geld, S. Jayatilleke, S. M. Jayatilleke, G. Mancinelli, B. T. Meadows, M. D. Sokoloff

University of Cincinnati, Cincinnati, OH 45221, USA

J. Blouw, J. L. Harton, M. Krishnamurthy, A. Soffer, W. H. Toki, R. J. Wilson, J. Zhang

Colorado State University, Fort Collins, CO 80523, USA

S. Fahey, W. T. Ford, F. Gaede, D. R. Johnson, A. K. Michael, U. Nauenberg, A. Olivas, H. Park, P. Rankin, J. Roy, S. Sen, J. G. Smith, D. L. Wagner

University of Colorado, Boulder, CO 80309, USA

T. Brandt, J. Brose, G. Dahlinger, M. Dickopp, R. S. Dubitzky, M. L. Kocian, R. Müller-Pfefferkorn, K. R. Schubert, R. Schwierz, B. Spaan, L. Wilden

Technische Universität Dresden, Inst. f. Kern- u. Teilchenphysik, D-01062 Dresden, Germany

L. Behr, D. Bernard, G. R. Bonneaud, F. Brochard, J. Cohen-Tanugi, S. Ferrag, E. Roussot, C. Thiebaux, G. Vasileiadis, M. Verderi

Ecole Polytechnique, Lab de Physique Nucléaire H. E., F-91128 Palaiseau, France

A. Anjomshoaa, R. Bernet, F. Di Lodovico, F. Muheim, S. Playfer, J. E. Swain

University of Edinburgh, Edinburgh EH9 3JZ, UK

C. Bozzi, S. Dittongo, M. Folegani, L. Piemontese

Università di Ferrara, Dipartimento di Fisica and INFN, I-44100 Ferrara, Italy

E. Treadwell

Florida A&M University, Tallahassee, FL 32307, USA

[1]Jointly appointed with Università di Roma La Sapienza, Dipartimento di Fisica and INFN, I-00185 Roma, Italy

R. Baldini-Ferroli, A. Calcaterra, R. de Sangro, D. Falciai, G. Finocchiaro, P. Patteri, I. M. Peruzzi,[2] M. Piccolo, A. Zallo

Laboratori Nazionali di Frascati dell'INFN, I-00044 Frascati, Italy

S. Bagnasco, A. Buzzo, R. Contri, G. Crosetti, P. Fabbricatore, S. Farinon, M. Lo Vetere, M. Macri, M. R. Monge, R. Musenich, R. Parodi, S. Passaggio, F. C. Pastore, C. Patrignani, M. G. Pia, C. Priano, E. Robutti, A. Santroni

Università di Genova, Dipartimento di Fisica and INFN, I-16146 Genova, Italy

J. Cochran, H. B. Crawley, P.-A. Fischer, J. Lamsa, W. T. Meyer, E. I. Rosenberg

Iowa State University, Ames, IA 50011-3160, USA

R. Bartoldus, T. Dignan, R. Hamilton, U. Mallik

University of Iowa, Iowa City, IA 52242, USA

C. Angelini, G. Batignani, S. Bettarini, M. Bondioli, M. Carpinelli, F. Forti, M. A. Giorgi, A. Lusiani, M. Morganti, E. Paoloni, M. Rama, G. Rizzo, F. Sandrelli, G. Simi, G. Triggiani

Università di Pisa, Scuola Normale Superiore, and INFN, I-56010 Pisa, Italy

M. Benkebil, G. Grosdidier, C. Hast, A. Hoecker, V. LePeltier, A. M. Lutz, S. Plaszczynski, M. H. Schune, S. Trincaz-Duvoid, A. Valassi, G. Wormser

LAL, F-91898 ORSAY Cedex, France

R. M. Bionta, V. Brigljević, O. Fackler, D. Fujino, D. J. Lange, M. Mugge, X. Shi, T. J. Wenaus, D. M. Wright, C. R. Wuest

Lawrence Livermore National Laboratory, Livermore, CA 94550, USA

M. Carroll, J. R. Fry, E. Gabathuler, R. Gamet, M. George, M. Kay, S. McMahon, T. R. McMahon, D. J. Payne, C. Touramanis

University of Liverpool, Liverpool L69 3BX, UK

M. L. Aspinwall, P. D. Dauncey, I. Eschrich, N. J. W. Gunawardane, R. Martin, J. A. Nash, P. Sanders, D. Smith

University of London, Imperial College, London, SW7 2BW, UK

D. E. Azzopardi, J. J. Back, P. Dixon, P. F. Harrison, P. B. Vidal, M. I. Williams

University of London, Queen Mary and Westfield College, London, E1 4NS, UK

G. Cowan, M. G. Green, A. Kurup, P. McGrath, I. Scott

University of London, Royal Holloway and Bedford New College, Egham, Surrey TW20 0EX, UK

D. Brown, C. L. Davis, Y. Li, J. Pavlovich, A. Trunov

University of Louisville, Louisville, KY 40292, USA

J. Allison, R. J. Barlow, J. T. Boyd, J. Fullwood, A. Khan, G. D. Lafferty, N. Savvas, E. T. Simopoulos, R. J. Thompson, J. H. Weatherall

University of Manchester, Manchester M13 9PL, UK

[2]Jointly appointed with Univ. di Perugia, I-06100 Perugia, Italy

C. Dallapiccola, A. Farbin, A. Jawahery, V. Lillard, J. Olsen, D. A. Roberts
University of Maryland, College Park, MD 20742, USA

B. Brau, R. Cowan, F. Taylor, R. K. Yamamoto
Massachusetts Institute of Technology, Lab for Nuclear Science, Cambridge, MA 02139, USA

G. Blaylock, K. T. Flood, S. S. Hertzbach, R. Kofler, C. S. Lin, S. Willocq, J. Wittlin
University of Massachusetts, Amherst, MA 01003, USA

P. Bloom, D. I. Britton, M. Milek, P. M. Patel, J. Trischuk
McGill University, Montreal, PQ, Canada H3A 2T8

F. Lanni, F. Palombo
Università di Milano, Dipartimento di Fisica and INFN, I-20133 Milano, Italy

J. M. Bauer, M. Booke, L. Cremaldi, R. Kroeger, J. Reidy, D. Sanders, D. J. Summers
University of Mississippi, University, MS 38677, USA

J. F. Arguin, J. P. Martin, J. Y. Nief, R. Seitz, P. Taras, A. Woch, V. Zacek
Université de Montreal, Lab. Rene J. A. Levesque, Montreal, QC, Canada, H3C 3J7

H. Nicholson, C. S. Sutton
Mount Holyoke College, South Hadley, MA 01075, USA

N. Cavallo, G. De Nardo, F. Fabozzi, C. Gatto, L. Lista, D. Piccolo, C. Sciacca
Università di Napoli Federico II, Dipartimento di Scienze Fisiche and INFN, I-80126 Napoli, Italy

M. Falbo
Northern Kentucky University, Highland Heights, KY 41076, USA

J. M. LoSecco
University of Notre Dame, Notre Dame, IN 46556, USA

J. R. G. Alsmiller, T. A. Gabriel, T. Handler
Oak Ridge National Laboratory, Oak Ridge, TN 37831, USA

F. Colecchia, F. Dal Corso, G. Michelon, M. Morandin, M. Posocco, R. Stroili, E. Torassa, C. Voci
Università di Padova, Dipartimento di Fisica and INFN, I-35131 Padova, Italy

M. Benayoun, H. Briand, J. Chauveau, P. David, C. De la Vaissière, L. Del Buono, O. Hamon, F. Le Diberder, Ph. Leruste, J. Lory, F. Martinez-Vidal, L. Roos, J. Stark, S. Versillé
Universités Paris VI et VII, Lab de Physique Nucléaire H. E., F-75252 Paris, Cedex 05, France

P. F. Manfredi, V. Re, V. Speziali
Università di Pavia, Dipartimento di Elettronica and INFN, I-27100 Pavia, Italy

E. D. Frank, L. Gladney, Q. H. Guo, J. H. Panetta
University of Pennsylvania, Philadelphia, PA 19104, USA

M. Haire, D. Judd, K. Paick, L. Turnbull, D. E. Wagoner
Prairie View A&M University, Prairie View, TX 77446, USA

J. Albert, C. Bula, M. H. Kelsey, C. Lu, K. T. McDonald, V. Miftakov, S. F. Schaffner, A. J. S. Smith, A. Tumanov, E. W. Varnes

Princeton University, Princeton, NJ 08544, USA

G. Cavoto, F. Ferrarotto, F. Ferroni, K. Fratini, E. Lamanna, E. Leonardi, M. A. Mazzoni, S. Morganti, G. Piredda, F. Safai Tehrani, M. Serra

Università di Roma La Sapienza, Dipartimento di Fisica and INFN, I-00185 Roma, Italy

R. Waldi

Universität Rostock, D-18051 Rostock, Germany

P. F. Jacques, M. Kalelkar, R. J. Plano

Rutgers University, New Brunswick, NJ 08903, USA

T. Adye, U. Egede, B. Franek, N. I. Geddes, G. P. Gopal

Rutherford Appleton Laboratory, Chilton, Didcot, Oxon., OX11 0QX, UK

N. Copty, M. V. Purohit, F. X. Yumiceva

University of South Carolina, Columbia, SC 29208, USA

I. Adam, P. L. Anthony, F. Anulli, D. Aston, K. Baird, E. Bloom, A. M. Boyarski, F. Bulos, G. Calderini, M. R. Convery, D. P. Coupal, D. H. Coward, J. Dorfan, M. Doser, W. Dunwoodie, T. Glanzman, G. L. Godfrey, P. Grosso, J. L. Hewett, T. Himel, M. E. Huffer, W. R. Innes, C. P. Jessop, P. Kim, U. Langenegger, D. W. G. S. Leith, S. Luitz, V. Luth, H. L. Lynch, G. Manzin, H. Marsiske, S. Menke, R. Messner, K. C. Moffeit, M. Morii, R. Mount, D. R. Muller, C. P. O'Grady, P. Paolucci, S. Petrak, H. Quinn, B. N. Ratcliff, S. H. Robertson, L. S. Rochester, A. Roodman, T. Schietinger, R. H. Schindler, J. Schwiening, G. Sciolla, V. V. Serbo, A. Snyder, A. Soha, S. M. Spanier, A. Stahl, D. Su, M. K. Sullivan, M. Talby, H. A. Tanaka, J. Va'vra, S. R. Wagner, A. J. R. Weinstein, W. J. Wisniewski, C. C. Young

Stanford Linear Accelerator Center, Stanford, CA 94309, USA

P. R. Burchat, C. H. Cheng, D. Kirkby, T. I. Meyer, C. Roat

Stanford University, Stanford, CA 94305-4060, USA

A. De Silva, R. Henderson

TRIUMF, Vancouver, BC, Canada V6T 2A3

W. Bugg, H. Cohn, E. Hart, A. W. Weidemann

University of Tennessee, Knoxville, TN 37996, USA

T. Benninger, J. M. Izen, I. Kitayama, X. C. Lou, M. Turcotte

University of Texas at Dallas, Richardson, TX 75083, USA

F. Bianchi, M. Bona, B. Di Girolamo, D. Gamba, A. Smol, D. Zanin

Università di Torino, Dipartimento di Fisica Sperimentale and INFN, I-10125 Torino, Italy

L. Bosisio, G. Della Ricca, L. Lanceri, A. Pompili, P. Poropat, M. Prest, E. Vallazza, G. Vuagnin

Università di Trieste, Dipartimento di Fisica and INFN, I-34127 Trieste, Italy

R. S. Panvini

Vanderbilt University, Nashville, TN 37235, USA

C. M. Brown, P. D. Jackson, R. Kowalewski, J. M. Roney

University of Victoria, Victoria, BC, Canada V8W 3P6

H. R. Band, E. Charles, S. Dasu, P. Elmer, J. R. Johnson, J. Nielsen, W. Orejudos, Y. Pan, R. Prepost, I. J. Scott, J. Walsh, S. L. Wu, Z. Yu, H. Zobernig

University of Wisconsin, Madison, WI 53706, USA

1 Introduction

This document presents two analyses designed to select large samples of B^0 mesons with inclusive reconstruction techniques. The first method finds $B^0 \to D^{*-}\pi^+$ events and the second $B^0 \to D^{*-}\ell^+\nu_\ell$; while the two techniques are different in detail, they both share the common feature of making no attempt to reconstruct the D^0 produced in the $D^{*-} \to D^0\pi^-$ decay, thereby achieving high efficiency comparing to the exclusive reconstruction.

Taking advantage of the boost of the $\Upsilon(4S)$ system at PEP-II, the lifetime of the B^0 meson is determined separately, with a good statistical precision, using both samples of events. Tagging the flavor of the second B^0 in the event will eventually also allow a measurement of the mixing parameter Δm_d.

1.1 $B^0 \to D^{*-}\pi^+$ inclusive reconstruction

The decay $B^0 \to D^{*-}\pi^+$ is interesting for many reasons, but particularly since it may exhibit *CP* violation [1]. Since the asymmetry is expected to be small, this is a long term goal and the first steps toward it are the measurement of the B_d^0 lifetime and mixing using this process.

The full reconstruction of the decay chain $B^0 \to D^{*-}\pi^+$, $D^{*-} \to \overline{D}^0\pi^-$, where the D^0 decays in the mode $\overline{D}^0 \to K^-\pi^+, K^-\pi^+\pi^0, K^-\pi^-\pi^+\pi^+, \overline{K}^0\pi^-\pi^+, ...$, allows one to evaluate detector performance and to extract the signal with an excellent signal over background ratio. However the loss in statistics is substantial and may limit a *CP* violation measurement given the small expected asymmetry.

An alternative approach exists for extracting the signal without reconstructing the decay of the D^0 meson. This partial reconstruction method has already been used successfully by other experiments [2, 3] and allows an increase of the size of the reconstructed sample by about an order of magnitude while maintaining the background at a reasonable level.

No attempt is made to reconstruct the D^0 decays. Therefore, one searches for a pair of oppositely-charged pions (π_f, π_s) and, assuming that their origin is a B^0 meson, calculates the missing invariant mass which should be the D^0 mass if our hypothesis was correct. Without the constraint of the D^0 mass, the direction of the B meson is unknown. Although its angle with respect to π_f direction can be deduced, the angle ϕ around this direction is undetermined. For more details see [2, 3].

Using the beam energy constraint, the missing mass, M_{miss}, is computed from the energy and momenta of the two reconstructed pions. Since this still depends on the unknown angle ϕ of the B^0 momentum, in this analysis, M_{miss} is defined as the average of the maximum and minimum value of M_{miss} over all ϕ angles.

A Monte Carlo study shows that the resolution on M_{miss} obtained in this way is of the order of $3\,\mathrm{MeV}/c^2$, and that it is dominated by the tracking precision for the measurement of the two pions.

1.2 $B^0 \to D^{*-}\ell^+\nu_\ell$ inclusive reconstruction

The B^0 semileptonic decay process $B^0 \to D^{*-}\ell^+\nu_\ell$ is characterized by high branching ratio and clear experimental signature. These facts allow the selection of large event samples with small background contamination. Therefore this process has been widely used in the past to determine several B^0 properties, along which its lifetime, τ_{B^0}, and the $B^0\overline{B}^0$ mass splitting, Δm_d [4]. In those measurements the D^{*-} particle was reconstructed through its decay $D^{*-} \to D^0\pi^-$, and

the D^0 was identified by means of exclusive reconstruction of a few final states which provide high selection efficiency and high background rejection.

Due to the restricted phase space of the $D^{*-} \to D^0\pi^-$ transition it is however possible to tag this process by reconstructing only the low energy charged pion (hereafter called π^*) from the D^{*-} decay, without reconstructing the D^0. This "inclusive" approach allows us to select an event sample about ten times more abundant than the exclusive analysis. This method has been extensively used in the past by the ARGUS and CLEO collaborations at the $\Upsilon(4S)$ to determine several B^0 and D^0 properties [5, 6], and by DELPHI and OPAL at LEP to measure $|V_{cb}|$ and the $B^0 \to D^{*-}\ell^+\nu_\ell$ branching fraction [7, 8]. Measurements of the B^0 lifetime and oscillation frequency with this approach have only been performed by the DELPHI collaboration at LEP [9, 10] and are, at present time, among the most precise determinations of those quantities.

2 Detector and data

The data used in this analysis were collected with the *BABAR* detector (for a detailed description see [11]) at the PEP-II storage ring. The statistics analyzed corresponds to an integrated luminosity of 7.9 (7.1) fb^{-1} of data collected on the $\Upsilon(4S)$peak, and 1.2 (1.0) fb^{-1} collected below peak, for the $B^0 \to D^{*-}\pi^+$ ($B^0 \to D^{*-}\ell^+\nu_\ell$) analysis. The off-resonance data were used for background study purposes.

Samples of about one million $B^0\overline{B}^0$ and B^+B^- simulated events were also analyzed; in addition, about 28000 (175000) $B^0\overline{B}^0$ were generated, were one of the B^0 mesons was forced to decay to $B^0 \to D^{*-}\pi^+$ ($D^{*-}\ell^+\nu$).

3 B^0 to $D^{*-}\pi^+$ analysis and results

3.1 Inclusive reconstruction of $B^0 \to D^{*-}\pi^+$

3.1.1 Track and signal selection

The fast and slow pion have been selected by requiring Drift Chamber (DCH) and Silicon Vertex Detector (SVT) quality cuts, respectively. In addition, the fast pion should have a momentum in the center of mass frame between 2.114 and 2.404 GeV/c, and should not to be identified as a muon or as an electron. The slow pion should have a momentum in the laboratory of at least 50 MeV/c. A further set of cuts were applied to reject electrons and kaons from the fast and slow pion tracks using the calorimeter and the Detection of Internally Reflected Cherenkov light (DIRC).

In order to obtain the signal, pairs of oppositely-charged tracks were required and the inclusive reconstruction method was applied, leading to a value for M_{miss}. An optimized selection criterium is necessary in order to reduce the combinatorial background, mainly from continuum events.

In order of decreasing discriminating power, the quantities used for signal selection are:

1. R_2, the normalized second Fox-Wolfram moment, is required to be less than 0.35.

2. Requiring that no other tracks be in a cone of opening angle 0.4 rad centered on the fast pion candidate momentum vector in the $\Upsilon(4S)$ system.

3. Two sets of particles are defined: all tracks and calorimeter clusters, excluding the fast and slow pion (SET1), and a set where all particles in a cone around the reference D^0 direction are also excluded (SET2) (see section 3.2.2). A single discriminating variable is constructed

using the Fisher method, based on 15 input variables. (For SET1, the scalar sum of the CM momenta of tracks and showers in nine 20^0 angular bins around the fast pion, and the sphericity. For SET2, the angle of the sphericity axis and the angle of the particle of highest energy with respect to the fast pion, and the combined mass and momentum of all the particles.)

4. The cosine of the helicity angle[1] is required to be larger than 0.4 in absolute value.

The efficiency for these cuts as determined using Monte Carlo simulation is 27.5%.

The distribution of the missing mass obtained on the data, applying only the R_2 cut, is shown in Fig. 1. The fitted signal is 10992 ± 235 events. Applying all the cuts (see also Section 6.4) the distribution in Fig. 2 is obtained, containing 1696 ± 107 events.

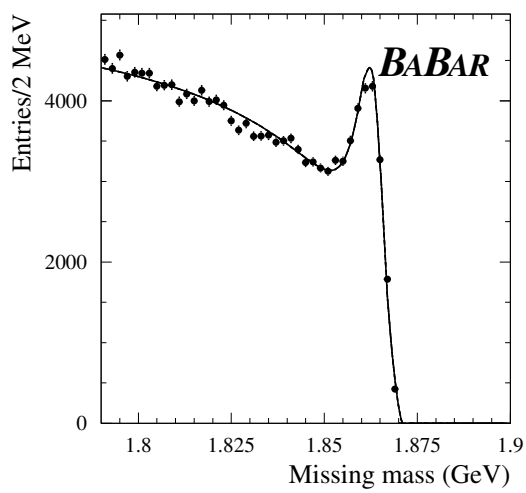

Figure 1: Missing mass distribution for partially reconstructed $B^0 \to D^{*-}\pi^+$ events from data. Here only the cut on R_2 is applied.

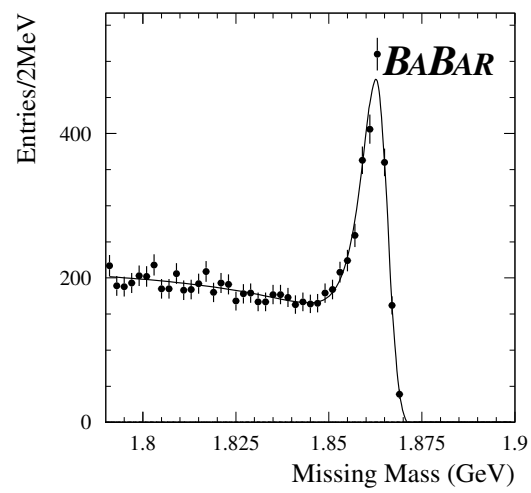

Figure 2: Missing mass distribution for partially reconstructed $B^0 \to D^{*-}\pi^+$ events from data after all the cuts are applied.

No peak is observed in the corresponding distribution for wrong charge combinations, nor in the off-resonance data.

3.1.2 Signal and background composition

Other B decay modes may produce an enhancement at the end of the missing mass spectrum in the same region where the signal is expected. An obvious example is the decay $B^0 \to D^{*-}\rho^+$.

To study this effect, we have fit separately the distribution obtained for generic B mesons and charged B mesons from Monte Carlo simulation. Contributions to the missing mass spectrum come from a) $B^0 \to D^{*-}\pi^+$ signal, b) combinations of a true soft pion from a D with a pion coming from a B^0 meson or from a direct ρ, c) combinations of a true soft pion with a direct lepton, and d) all other combinations. Only the categories a), b) and c) show clearly a peak at the end of the spectrum. The fit gives 461 ± 26 events, which is consistent with the sum of the contribution

[1]angle between the soft pion and the D^* flight direction in the rest frame of the latter

from a) (365 events) and b) (100 events). Therefore, we estimate that the signal contribution is enhanced by 26% from other B^0 decay modes.

No clear peaking is observed for charged B mesons. The estimate for their fraction in the signal sample is $6.0 \pm 3.1\%$.

Figure 3 shows a comparison between data and Monte Carlo distributions for missing mass, after all cuts. The Monte Carlo is normalized to the data.

Table 1: Contribution (in %) of different background components in the sideband, signal region and for the wrong-charge combination for the (π_f, π_s) pair.

component	sideband	signal	wrong charge
$q\overline{q}$, $q = u, d, s$	40.9	17.9	40.8
$c\overline{c}$	17.4	30.6	19.1
B^+B^- generic	24.3	28.2	21.3
$B^0\overline{B}^0$ generic	17.4	23.3	18.8

For the lifetime measurement, the combinatorial background parameters have been fitted to the data for wrong-charge combinations with $M_{miss} > 1.84\,\mathrm{GeV}/c^2$. As a cross-check, a sideband region ($1.8 < M_{miss} < 1.84\,\mathrm{GeV}/c^2$) is also defined. The signal region is taken to be the interval $M_{miss} > 1.854\,\mathrm{GeV}/c^2$. The fractions of the different components in the sideband, signal and wrong charge region are shown in Table 1.

3.2 Lifetime measurement

3.2.1 $B^0 \to D^{*-}\pi^+$ vertex determination

The $B^0 \to D^{*-}\pi^+$ vertex has been computed fitting the fast and slow pion tracks with the beam spot constraint. To take into account the flight of the B meson in the xy plane, the effective size of the luminous region in the vertical direction has been assumed to be $60\,\mu$m.

The resolution on the $B^0 \to D^{*-}\pi^+$ vertex is dominated by the beam spot and by the fast pion track. Therefore, we have required the fast pion to have at least 3 SVT hits. The longitudinal or z precision on this vertex is strongly correlated to the direction of the fast pion track and is best when this direction lies in the transverse plane, in which case the resolution is $50\,\mu$m. The error on the z coordinate of this vertex is required to be less than $150\,\mu$m. The z resolution of the $B^0 \to D^{*-}\pi^+$ vertex can be fitted with the sum of two Gaussian distributions, where the core Gaussian has a width of $48\,\mu$m and contains 80% of the events.

3.2.2 Rejection of D^0 tracks and B_{tag} vertex determination

Before fitting the vertex of the second B in the event, hereafter named B_{tag}, it is necessary to reject tracks coming from the non-reconstructed D^0. Including these tracks in the fit would result in a bias, pulling the position of the B_{tag} vertex systematically closer to the $B^0 \to D^{*-}\pi^+$ vertex and thereby reducing the measured lifetime. Thanks to the high momentum of the D^0, most of its decay products will be boosted in a cone around the parent direction. To reject these, tracks are excluded that lie within the region in the $\theta_{TK} - p$ plane that is populated by D^0 decay particles, where θ_{TK} is the the angle between the direction of a given track and the reconstructed D^0 direction and p is the momentum of the track in the center of mass frame. This requirement is applied up to a

maximum angle of 2 rad. It has an efficiency of 45% for the tracks from the B_{tag} and 1.8% for the D^0 decay products. As a result, 98% of the accepted tracks come from the B_{tag}.

The B_{tag} vertex has been fitted from the tracks selected as explained above, discarding the tracks with excessive contribution to χ^2. To achieve a high quality vertex it is required that the fit be performed using at least two tracks. Even after this treatment, some tracks from the decay of charmed hadrons are still included in the B_{tag} vertex fit. As these come from the charm decay vertex, which is generally at larger z values due to the charm hadron lifetime and the boost in the laboratory frame, this produces a bias in the mean value of the z coordinate of the order of $20\,\mu$m. The z resolution for the B_{tag} vertex can be fit with the sum of two Gaussian distributions, where the core Gaussian has a width of $92\,\mu$m and it contains 70% of the events.

3.2.3 Vertex quality selection

Further selection cuts are applied to improve the vertex quality. The number of SVT hits associated to the fast pion is required to be at least 4, the z error on the $B^0 \to D^{*-}\pi^+$ vertex fit is required to be less than $150\,\mu$m, the normalized χ^2 of the $B^0 \to D^{*-}\pi^+$ vertex fit is required to be less than 20, and at least two tracks are required to be used by the B_{tag} vertex fit. The efficiency for these cuts estimated from Monte Carlo simulation to be 58%. The number of signal events is 1696 ± 107 and the fraction of combinatorial background in the signal region α_{back} is $27 \pm 6\%$.

3.2.4 B^0 lifetime fit

Using the fit result for the two B vertices, it is possible to extract a longitudinal vertex separation, $\Delta z = z_{D^*\pi} - z_{tag}$. Δt is then computed using the approximation $\Delta t = \Delta z/\beta\gamma c$, where the boost $\beta\gamma$ of the $\Upsilon(4S)$ at PEP-II is known to be 0.56. In order to fit the Δt distribution, three regions were defined in the M_{miss} spectrum: a signal region for candidates with $M_{miss} > 1.854\,\mathrm{GeV}/c^2$, a sideband region with $1.800 < M_{miss} < 1.840\,\mathrm{GeV}/c^2$ and a wrong charge region for candidates with both pions have the same charge and $M_{miss} > 1.840\,\mathrm{GeV}/c^2$.

The wrong-charge distribution is used to define the shape of the combinatorial background under the signal. The Δt distribution of the wrong charge region is fit with the function:

$$\begin{aligned} f_b(\Delta t) = (1-\alpha_B)(\alpha_{uds}\, gauss(\Delta t, \sigma_{uds}) + (1-\alpha_{uds})\, gauss(\Delta t, \sigma_c)) \\ +\alpha_B((1-\alpha_{bw})E_G(\Delta t - b_n; \tau_{back}, \sigma_{bn}) + \alpha_{bw} E_G(\Delta t - b_w; \tau_{back}, \sigma_{bw})) \end{aligned} \quad (1)$$

where $E_G(t;\tau,\sigma)$ is the convolution of an exponential with lifetime τ with a gaussian of width σ.

The parameters α_{bw}, b_n, σ_{bn}, b_w, σ_{bw} for the background "resolution function" are fixed to the resolution function determined from Monte Carlo simulation for signal events. The background lifetime is fixed to the value, 1.55 ps, measured from the same distribution for $B\overline{B}$ events in the Monte Carlo sample. The widths σ_{uds} and σ_c of the two Gaussian distributions used to parametrise the continuum light quark (uds) and charm components are fixed to the values, 0.70 and 0.96 ps respectively, extracted from the Monte Carlo. α_B and α_{uds} are the only parameters left free in the fit of the background Δt distribution.

To take into account the fact that the fractions of uds and charm in the different samples are different (cf. table 1), α_{uds} is fixed to the value 0.37, obtained from the Monte Carlo simulation in the signal region, for the final lifetime fit.

The lifetime fit is performed using an event-by-event resolution estimate obtained by scaling the error given by the vertex fit for the two vertices. The Monte Carlo Δz pull distribution has been

used for the rescaling. This can be described by two Gaussian distributions with widths $p_n = 1.04$ and $p_w = 2.51$, centered at $s_n = -0.22$ and $s_w = -0.95$ respectively. The fraction α_{wide} of the events in the wide Gaussian is 11%.

Therefore, the probability density function for the unbinned maximum likelihood fit for event i is:

$$f(\Delta t_i, \sigma_i) = (1 - \alpha_{back}) f_s(\Delta t_i, \sigma_i) + \alpha_{back} f_b(\Delta t_i) \tag{2}$$

where

$$f_s(\Delta t_i, \sigma_i) = (1 - \alpha_{wide}) E_G(\Delta t_i - s_n \sigma_i; \tau_{B^0}, S p_n \sigma_i) + \alpha_{wide} E_G(\Delta t_i - s_w \sigma_i; \tau_{B^0}, S p_w \sigma_i) \tag{3}$$

Here Δt_i and σ_i are Δt and its error coming from the fit of the two B vertices and S is a global scale factor for the errors.

The result of the unbinned maximum likelihood fit with one free parameter, the B^0 lifetime, is $\tau_{B^0} = 1.51 \pm 0.05$ ps as shown in Fig 4.

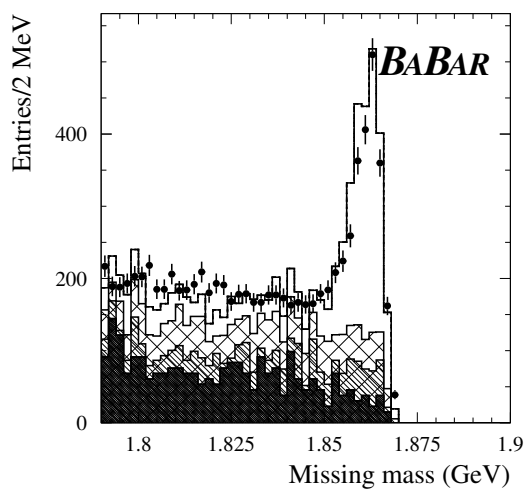

Figure 3: Missing mass distribution in partially reconstructed $B^0 \to D^{*-}\pi^+$ events after all cuts. The data are represented by points. The contribution of the $q\overline{q}$ final states from Monte Carlo is: uds (black), c (dense hatched), charged B (light hatched), neutral B (white).

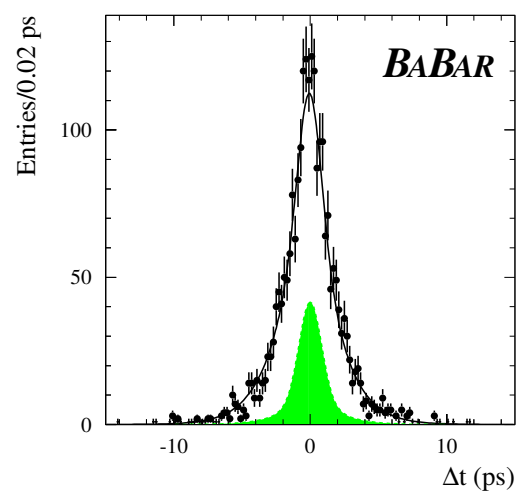

Figure 4: Distribution of Δt in ps. The data are represented by the points with error bars. The continuous line shows the result of the fit and the shaded area shows the contribution of the combinatorial background (27% of the sample).

3.2.5 Bias

Using the same procedure, a lifetime fit has been performed on a signal Monte Carlo sample, giving $\tau_{B^0} = 1.48 \pm 0.025$ ps. Removing the tracks from the D^0, the bias is removed and the result, $\tau_{B^0} = 1.52 \pm 0.02$ ps, is compatible with the generated lifetime $\tau_{B^0} = 1.56$ ps. The estimated bias is then 0.04 ps and this has been added to the fit result from data to obtain the quoted final lifetime value.

Table 2: Results of the fit obtained with different values for the cone cut for a smaller data sample corresponding to 5.3 fb^{-1} after applying the Monte Carlo bias correction. All the times are in ps.

Cut (rad)	Events	τ_{raw}	$\Delta\tau_{MC}$	τ_{corr}
1	2595	1.42 ± 0.04	0.12 ± 0.02	1.54
1.5	1839	1.49 ± 0.05	0.06 ± 0.02	1.55
2	1287	1.52 ± 0.06	0.04 ± 0.02	1.56

Table 3: Sources of the systematic error and their impact on τ.

Source	Variation	$\Delta\tau$ (ps)
α_{back}	$27 \pm 6\%$	0.039
α_B	$49 \pm 3\%$	0.012
α_{uds}	$37 \pm 20\%$	0.006
τ_{back}	$1.55 \pm 0.05\ ps$	0.010
S	1.00 ± 0.13	0.051
bias	0.04 ± 0.02	0.020
Total	-	0.07

Table 2 shows the fit results obtained with different values for the cone cut, after applying the appropriate Monte Carlo correction for bias. The corrected lifetime is stable with respect to the variation of the cone cut.

3.2.6 Systematics

A preliminary evaluation of the systematic errors on the lifetime result has been performed.

The combinatorial background fraction α_{back} has been varied by 6% leading to a variation of 0.039 ps in the fitted lifetime. The parametrisation of the combinatorial background has been varied yielding variations of 0.012 (α_B $B\overline{B}$ fraction), 0.006 (α_{uds} uds fraction) and 0.010 ps (τ_{back} background lifetime).

This analysis relies on the resolution function fit from the Monte Carlo simulation and therefore is sensitive to possible discrepancies between simulation and data. The global scale factor S has been left free in the fit giving $S = 1.13 \pm 0.12$. The corresponding variation of the lifetime of 0.051 ps has been added to the systematic error.

The total systematic uncertainty of 0.07 ps, is dominated by the uncertainty in the continuum background fraction and the uncertainty in the vertex resolution function (table 3). As these two contributions are related to variations estimated on the data themselves, further increases in the size of the data sample should reduce these systematic errors.

As a further cross-check of the resolution in Δz, a data-Monte Carlo comparison has been performed for the sideband and for the off resonance data. The agreement is good in both cases.

4 B^0 to $D^* \ell \bar{\nu}_\ell$ analysis and results

4.1 Event and track selection and sample composition

4.1.1 $B\overline{B}$ event selection

Hadronic events were selected by requiring that at least four charged tracks be present. To reduce the contamination from light quark and $c\overline{c}$ events, the second Fox-Wolfram moment R_2 is required to be smaller than 0.5.

4.1.2 Track selection

Only charged particles tracks were employed for this analysis. High momentum tracks were reconstructed by matching hits in the Silicon Vertex Tracker (SVT) with track elements in the Drift Chamber (DCH). Low momentum tracks do not hit enough wires in the DCH due to the bending induced by the magnetic field. They are however reconstructed by the SVT stand-alone pattern recognition, with more than 50% efficiency for momentum $p > 70\,\mathrm{MeV}/c$.

4.1.3 Particle identification

Charged tracks are identified as electrons using information from the electromagnetic calorimeter (ratio of the energy released to the associated track momentum, transverse profile of the electromagnetic shower), from the energy loss in the DCH and from the Cerenkov angle as measured with the Detector of Internally Reflected Cherenkov light (DIRC). The efficiency for electron identification in the acceptance of the electromagnetic calorimeter is about 90%, with a hadron mis-identification probability $< 1\%$.

Muons were selected by requiring penetration through most of the Instrumented Flux Return (IFR). The selection requirements result in $\sim 75\%$ efficiency for muon identification with $\sim 2\%$ hadron mis-identification probability. The Cherenkov light information in the DIRC was then employed to further reject mis-identified kaons, by requiring the likelihood for the kaon hypothesis to be less than five percent.

Kaons are used for B^0 flavour tagging. Among all charged particles with momentum $p > 500\,\mathrm{MeV}/c$, kaon candidates are selected on the basis of the energy loss in the DCH and in the SVT, as well as observed Cherenkov angle and number of photons in the DIRC. True kaons were selected with ~ 80 % efficiency, while $\sim 1\%$ of the pions were mis-identified as kaons.

4.1.4 $B^0 \to D^{*-}\ell^+\nu_\ell$ sample selection

Only the charged pion and the lepton are required to reconstruct $B^0 \to D^{*-}\ell^+\nu_\ell$ decays. The lepton candidate is required to have momentum in the $\Upsilon(4S)$ rest frame (k^*) in the range $1.4 < k^* < 2.3\,\mathrm{GeV}/c$, while the π^* had to satisfy the requirement $k^* < 190\,\mathrm{MeV}/c$.

Events were then selected by exploiting the kinematics of the decay. The B^0 four momentum is computed by assuming that the B^0 is produced at rest in the $\Upsilon(4S)$ decay, thereby neglecting the small boost of the B meson in this frame, where its momentum is about $300\,\mathrm{MeV}/c$. Due to the limited phase space available in the decay $D^{*-} \to D^0\pi^-$, the π^* is emitted inside a fairly restricted cone centered about the D^{*-} direction in the laboratory frame. The D^{*-} four-momentum can therefore be computed by approximating its polar and azimuth angles with those for the π^* , and

parametrising its momentum as a linear function of the π^* momentum:

$$p(D^{*-}) = \alpha + \beta \cdot p(\pi^*) \tag{4}$$

The D^{*-} direction is determined with an accuracy of about 15°, the error on the D^{*-} momentum is about 400 MeV/c. The neutrino escapes detection, but its invariant mass can be computed from the B^0, D^{*-} and ℓ^+ four-momenta from the relation:

$$M_\nu{}^2 = (\mathcal{P}(B^0) - \mathcal{P}(D^{*-}) - \mathcal{P}(\ell^+))^2 \tag{5}$$

Neglecting resolution effects, this quantity must be zero, while background events are spread over a wide range of M_ν^2.

The B^0 decay point is determined by intersecting the π^* and ℓ^+ tracks, constrained to the beam-spot position, which was determined on a run-by-run basis using Bhabha events. Only events for which the probability of the vertex fit was greater than 1% were further considered. This cut rejected about two thirds of the combinatorial background, while still retaining $\sim$ 80% of the signal.

4.1.5 Sample composition

The combinatorial background is determined from the data using those events for which the ℓ and π^* have same electric charge ("wrong-charge"). The contribution of the events from any decay process of the kind $B \to D^{*-}\ell^+\nu X$ ("resonant events") in the mass band ($M_\nu{}^2 > -2\,\mathrm{GeV}^2/\mathrm{c}^4$) was determined by subtracting the wrong-charge from the right-charge sample, normalized in the sideband region $-10 < M_\nu{}^2 < -5\,\mathrm{GeV}^2/\mathrm{c}^4$. A small correction ($\sim$ 5%) was applied to the wrong-charge on-peak events to account for events of the kind $B^0 \to \ell$, $\overline{B}^0 \to D^*$, which populates the right- and wrong-charge samples differently. The number of events obtained in the $\Upsilon(4S)$ resonance data sample is reported in the first line of Table 4. The second line shows the number of events obtained in the continuum data sample, multiplied by the ratio of the resonant and continuum luminosities: non $B\bar{B}$ events account for about 15% of the combinatorial background in the mass band and 5% of the sample obtained after subtraction of the combinatorial.

Table 4: Data statistics. The number of continuum events is normalized by the ratio of integrated luminosities.

Data Sample	Total	Resonant
On-peak	190080	89360
Off-Peak	23900	4160

In the Monte Carlo simulation the difference between the right charge and the rescaled wrong charge events in the mass band is $-2.1 \pm 1.6\%$ No correction is applied to the data for this effect, and a relative systematic error of $\pm 2\%$ is assumed. The number of resonant events in the sample is therefore:

$$\mathcal{N}_{res} = 89360 \pm 500 \text{ stat.} \pm 1800 \text{ syst.} \tag{6}$$

Figure 5 shows the M_ν^2 distribution for the electron data sample after subtraction of the off-peak data, before (left) and after (right) subtracting the combinatorial background.

Several physical processes contribute to the $D^*\ell\nu$ final state. Contamination from B^+ is mostly due to the decay $B^+ \to D^{**0}\ell\nu$ where the orbital charm excited state, D^{**0}, decays into

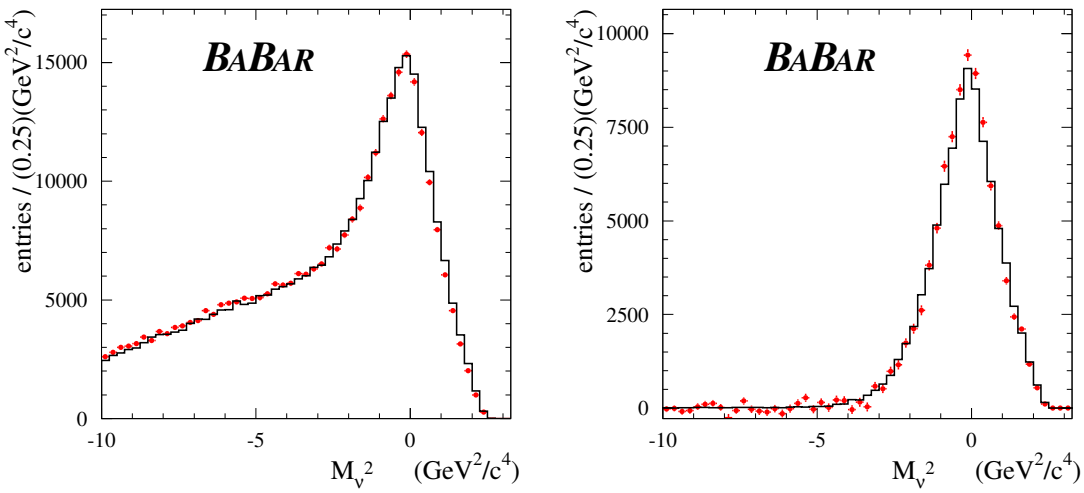

Figure 5: M_ν^2 distribution for the right charge data, after subtraction of the off-peak events for electron candidates. Dots with error bar: data; histogram: Monte Carlo simulation. The right hand side plot is obtained after subtraction of the combinatorial background.

$D^{*-}\pi^+$. The fraction of these events is 9±5%, where the error includes the systematic uncertainty due to the efficiency of the $B \to D^{**}\ell^+\nu_\ell$ selection. The composition of the sample is reported in Table 5. All the processes originating from a B^0 decay are considered as signal for this analysis.

Table 5: Sample Composition in the signal region (in %).

$B^0 \to D^{*-}\ell^+\nu_\ell$	36.6
$\overline{B}^0 \to D^{**}$	2.7
$\overline{B}^0 \to D^{*-}X_c/\tau$	0.4
$B \to D^{*-} fake\ l$	0.8
$B^+ \to D^{**}$	4.5
off-peak resonant	2.4
D^*/l from different Bs	4.0
Other $B\bar{B}$ Combinatorial	40.7
continuum	7.9

4.2 τ_{B^0} measurement and mixing

4.2.1 Proper time determination

The position of the $B^0 \to D^{*-}\ell^+\nu_\ell$ ("decay") vertex is reconstructed as described above from the ℓ, π^* tracks and the beam spot. The decay point of the other B ("tag" vertex) is determined using the remaining tracks in the event, constrained to the decay vertex in the plane orthogonal to the beam axis (x, y). This constraint exploits the fact that in the x-y view the separation between

the B^0 and the $\overline{B}^0$ is small compared to the experimental resolution; it is applied to remove the tracks from charm or hyperon decay from the vertex fit, which would bias the Δz reconstruction. To reduce the additional bias, peculiar to inclusive analyses, due to the un-resolved particles from the D^0 produced at the decay vertex, all the tracks lying within a one radian cone around the π^* are rejected from the tag vertex fit. In this way, about 60% of the D^0 tracks are removed, while still retaining $\sim 70\%$ of the B tag tracks.

The B^0 lifetime is determined by measuring event by event the distance along z between the decay and the tag vertex, as already described in section 3.2.4.

In the Monte Carlo simulation the Δz resolution for the signal events is described by two Gaussian distributions: the narrow (wide) component containing about 65% (35%) of the events, with a width of 120 (370) μm and a small bias of about 20 (65) μm. The pull distribution is parametrised by the sum of two Gaussian distributions, the narrow (wide) component contained 82% (18%) of the events, with a width of 1.07 (2.4) and a bias of 0.19 (0.7). The same resolution was assumed for B^+ events.

4.2.2 Determination of τ_{B^0}

The B^0 lifetime is determined by means of an unbinned maximum likelihood fit, accounting for the event-by-event error determined by the vertex reconstruction algorithm. The fit function was the sum of the probability density function (pdf) for B^0, B^+ and combinatorial background multiplied by the relative fractions for each type in the sample.

The Δz probability density function for B^0 events is described by the convolution of the proper time exponential with the pull resolution function described above. The same function is assumed for B^+ events, with a lifetime fixed to the present world average $\tau_{B^+} = 1.65 \pm 0.04$ ps.

The combinatorial background is described by the sum of a zero-lifetime and a non-zero lifetime component, both convoluted with a double Gaussian resolution function. All parameters (lifetime and fraction of non-zero lifetime events, widths, fractions and biases of the resolution function) were determined independently in the data and in the simulation by fitting wrong-charge events with the same program used to determine τ_{B^0}. Good consistency is found in the data and in the simulation, except for the rms width of the resolution function, which is 1.06 times larger in data. This discrepancy is attributed to resolution effects.

The method was first tested on the dedicated sample of simulated $B^0 \to D^{*-}\ell^+\nu_\ell$ events after applying the selection requirements described above. Due to the influence of the residual tracks from the un-reconstructed D^0, the measured lifetime in Monte Carlo is smaller than the generated one. The resulting reconstruction bias $\Delta\tau = 0.217 \pm 0.010$ ps for the lifetime is defined as the difference between the generated value of 1.560 ps and the fitted value ${\tau_{B^0}}^{raw,MC} = 1.343 \pm 0.010$ ps.

The final lifetime result for the data τ_{B^0} was obtained by adding the bias $\Delta\tau$ determined previously in the Monte Carlo to the raw fit result ${\tau_{B^0}}^{raw,Dt} = 1.405 \pm 0.016$ ps. The lifetime obtained in this way is:

$$\tau_{B^0} = 1.622 \pm 0.016 \text{ ps} \tag{7}$$

where the error is statistical only. Figure 6 shows a comparison between the data and the fit result.

4.3 Systematic studies

The study of the systematic effects is still preliminary. The following sources of error have been considered:

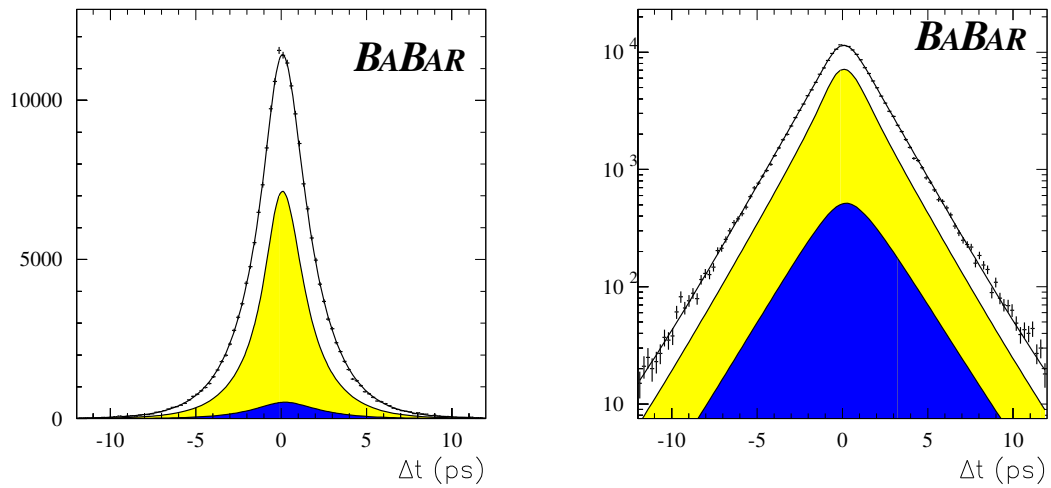

Figure 6: Lifetime fit result on a linear (left) and a logarithmic scale (right). The inner dark area is the B^+ contribution, the lighter area is the combinatorial background, the line is the result of the fit. Dots with error bars represent the data.

- **Sample Composition.** The amount of B^+ is varied by $\pm 50\%$; the fraction of combinatorial background is varied by ± 2 % according to the study described in Section 4.1; the fractions of events from uncorrelated ℓ D^{*-} production falling in the right- and wrong-charge samples are also varied within their allowed range, as computed from the measurements of the branching ratios $\mathcal{B}(B \to \ell X)$, $\mathcal{B}(B \to D^{*-} X)$, and of the $B^0 \overline{B}^0$ mixing parameter χ_d.

- **Background Lifetime.** The B^+ lifetime is varied within its error; the parameters of the pdf representing the combinatorial background is varied within their allowed range, properly accounting for correlations: this gives an error of ± 0.02 ps. Alternatively, the background parameters determined from a fit to the data side band are used, and the difference in the result ($+0.07$ ps) is added in quadrature to the systematic error.

- **Resolution Effects.** The fit was repeated by scaling the resolution function in the data by the factor 1.06 as indicated by the fit to the background sample: the measured lifetime decreased by 0.06 ps. This difference is considered as the systematic error due to the detector resolution. If the fraction of events in the narrow Gaussian describing the resolution function were varied by $\pm 5\%$ the fit result would vary by ± 0.04 ps. This is currently taken as a rough estimate of error for the pdf in data. The stability of the result versus some relevant variables ($\theta_{\ell,\,\mathrm{ps}}, \phi_{\ell,\,\mathrm{ps}}, p_{\ell,\,\mathrm{ps}}, {M_\nu}^2$) was also studied, but no significant effect was found.

- **Analysis Bias.** The sizeable correction for bias is determined from the Monte Carlo simulation. In the data, the fit was repeated for different values of the π^* cone cut. The systematic error was computed as half the difference between the largest and the smallest values obtained.

Table 6 shows the components of the estimated systematic error.

Table 6: Contributions to the estimated systematic error.

Source	Variation	$\sigma(\tau_{B^0})$ ps
B^+ fraction	$\pm 50\%$	∓ 0.005
$B \to D^{*-}, \bar{B} \to \ell$		± 0.002
Comb. frac.	$\pm 2\%$	± 0.014
Background pdf		$^{+0.070}_{-0.020}$
$\tau(B^+)$	± 0.04ps	± 0.005
Error Scale	1.06	-0.060
Data pdf	$\pm 5\%$	± 0.040
$\Delta\tau$		± 0.033
Total		$^{+0.091}_{-0.085}$

5 Summary

A large sample of $B^0 \to D^{*-}\pi^+$ and $B^0 \to D^{*-}\ell^+\nu_\ell$ decays has been obtained from the data sample collected by the *BABAR* detector at the PEP-II storage ring by means of partial D^{*-} reconstruction. Only the low energy π^- from the decay $D^{*-} \to \pi^- D^0$ was tagged and coupled to a high momentum opposite charge particle, either a pion or a lepton.

In the $B^0 \to D^{*-}\pi^+$ case, the missing mass recoiling against the system of the two pions was determined using the beam energy constraint. A clear excess of 10922 ± 235 events in the D^0 mass range was observed, and interpreted as the signal of $B^0 \to D^{*-}\pi^+$ production.

Events from the $B^0 \to D^{*-}\ell^+\nu_\ell$ three body decay were selected by reconstructing the mass of the un-observed neutrino: for this purpose, the B^0 four momentum was computed neglecting its small boost from the $\Upsilon(4S)$ decay, and the D^{*-} four momentum was computed by properly parametrising the one of the soft pion. A signal of $(89.4 \pm 0.5\text{stat.} \pm 1.8\text{syst.}) \times 10^3$ events was observed.

The lifetime of the B^0 meson was determined from the distance, projected along the beam direction, between the tagged and the recoil B^0 meson in the event. The preliminary results are:

$$\begin{aligned} \tau_{B^0} &= 1.55 \pm 0.05 \pm 0.07\,\text{ps} \quad (D^*\pi), \\ \tau_{B^0} &= 1.62 \pm 0.02 \pm 0.09\,\text{ps} \quad (D^*\ell\nu), \end{aligned}$$

were obtained by the two analyses. The two values are in good agreement, while the mutual correlation is small.

Preliminary studies indicate sufficient tagging efficiency and flavor separation for a time dependent measurement of the B^0 mixing process. Clear evidence of a time dependent asymmetry is observed in the data, consistent with the expectation from the simulation. This will allow a precise determination of the $B^0\overline{B}^0$ mass difference Δm_d in the future.

Acknowledgments

We are grateful for the contributions of our PEP-II colleagues in achieving the excellent luminosity and machine conditions that have made this work possible. We acknowledge support from the

Natural Sciences and Engineering Research Council (Canada), Institute of High Energy Physics (China), Commissariat à l'Energie Atomique and Institut National de Physique Nucléaire et de Physique des Particules (France), Bundesministerium für Bildung und Forschung (Germany), Istituto Nazionale di Fisica Nucleare (Italy), The Research Council of Norway, Ministry of Science and Technology of the Russian Federation, Particle Physics and Astronomy Research Council (United Kingdom), the Department of Energy (US), and the National Science Foundation (US). In addition, individual support has been received from the Swiss National Foundation, the A. P. Sloan Foundation, the Research Corporation, and the Alexander von Humboldt Foundation. The visiting groups wish to thank SLAC for the support and kind hospitality extended to them.

References

[1] The BABAR Collaboration, D. Boutigny et al, The *BABAR* Physics Book, SLAC-R-504, 1998, p. 481.

[2] ARGUS Collaboration, H. Albrecht *et al.*, Phys. Lett. **B182** (1986) 95

[3] CLEO Collaboration, G. Brandenburg *et al.*, Phys. Rev. Lett. **80** (1998) 2762

[4] For a complete review, see "Combined results on b-hadron production rates, lifetimes, oscillations and semileptonic decays", CERN-EP-2000-096, SLAC-PUB-8492, and references therein.

[5] ARGUS Collaboration, H. Albrecht *et al.*, Phys. Lett. **B322** (1994) 249.

[6] CLEO Collaboration, J. Bartelt *et al.*, Phys. Rev. Lett. **71** (1993) 1680.

[7] DELPHI Collaboration, P. Abreu *et al.*, Z. Phys. **C71** (1996) 539.

[8] OPAL Collaboration, G. Abbiendi *et al.*, Phys. Lett. **B482** (2000) 15.

[9] DELPHI Collaboration, P. Abreu *et al.*, Z. Phys. **C74** (1997) 19.

[10] DELPHI Collaboration, P. Abreu *et al.*, Z. Phys. **C76** (1997) 207.

[11] *BABAR* Collaboration, "*BABAR* Technical Design Report", D. Boutigny *et al.*, SLAC-R-95-457, March 1995; *BABAR* Collaboration, B. Aubert, *et al.*, "The *BABAR* experiment at PEP-II", *BABAR*-CONF-00/17, submitted to the XXXth International Conference on High Energy Physics, Osaka, Japan.

[12] *BABAR* Collaboration, B. Aubert *et.al.*, "Measurement of the time dependence of $B^0\overline{B}^0$ oscillations using inclusive dilepton events", *BABAR*-CONF-00/10, submitted to the XXXth International Conference on High Energy Physics, Osaka, Japan.